RESEARCH ARTICLE

Macromolecular Materials and Engineering
Open Access
www.mame-journal.de

Bio-Based Gradient Composites for 3D/4D Printing With Enhanced Mechanical, Shape Memory, and Flame-Retardant Properties

*Mohammadreza Lalegani Dezaki, Callum Branfoot, Jon Baxendale, and Mahdi Bodaghi**

This study explores the 3D/4D printing of polylactic acid (PLA) composites reinforced with natural particles from mussels PLA (MPLA) and wheat PLA (WPLA) using fused filament fabrication (FFF). The study employs functionally graded (FG) and multi-material (MM) printing processes emphasizing biodegradable and bio-derived materials. Shape memory polymer composites (SMPCs) with various MM and FG combinations are printed and examined. The microstructure, mechanical properties, flammability, and shape memory characteristics of these SMPCs are evaluated. The findings demonstrate that incorporating mussel and wheat particles enhances the mechanical performance of PLA, with a reduced burning rate compared to pure PLA samples. A sandwich FG composite structure shows superior strength in compression, tensile, and three-point bending tests, with WMWFG samples exhibiting a 106% increase in tensile strength compared to WPLA samples. The shape recovery and fixity of the 4D-printed SMPCs are investigated and WPLA specimens reveal the highest shape recovery ratio of ≈ 93.3% ± 1%. These findings highlight the potential of 4D-printed SMPCs for diverse applications, spanning shape morphing, human-material interaction, and mechanical engineering. Additionally, the research contributes to sustainability by promoting reduced material consumption and waste generation, as demonstrated by creating reusable and lightweight objects such as miniature pots, cutlery, holders, grippers, and wrappers.

1. Introduction

Fused filament fabrication (FFF) 4D printing constitutes a significant innovation in the field of additive manufacturing.[1,2] This method leverages the established principle of depositing composite materials in successive layers to create 3D objects.[3,4] This technology facilitates the development of dynamic functionally graded (FG) structures. These structures possess the remarkable capability to undergo modifications in both shape and internal arrangement upon exposure to predetermined environmental stimuli.[5,6] This innovation enables the programming of composite materials to exhibit transformative properties over time. Shape memory polymer composites (SMPCs) are frequently utilized in the fabrication of 4D-printed FG structures and actuators.[6–8] These materials exhibit a dynamic capacity to adjust their shape and configuration gradually, rendering them indispensable elements in the creation of functional and versatile designs.[9,10]

The range of materials that can be used with 3D printing or 4D printing has increased due to recent advancements in material science, particularly customized and printed composite materials.[11,12] FG composites are novel classes of materials possessing distinct properties in various regions due to gradual compositional and structural changes across their volume. Numerous forms of FG examples are present in nature, such as the morphological changes in bones and the tissue differences in seashells and bamboo shoots.[13,14] For this reason, FG materials are very interesting for a wide range of applications.[15,16] The distribution of multiple materials in FG composites eliminates clear boundaries, thus preventing issues like delamination or cracks that arise from abrupt changes in material composition and properties. This approach enables the achievement of multifunctional properties within the material.[17,18]

While integrating thermoplastic such as polylactic acid (PLA) with FFF offers benefits like affordability and straightforward printing, their mechanical strength and overall functionality can be limited.[19–21] 4D printing of FG biocomposites is a way to improve the strength and other mechanical properties of polymers made using FFF printing.[22–24] Incorporating reinforcement like

M. Lalegani Dezaki, M. Bodaghi
Department of Engineering, School of Science and Technology
Nottingham Trent University
Nottingham NG11 8NS, UK
E-mail: mahdi.bodaghi@ntu.ac.uk
C. Branfoot, J. Baxendale
Engineering Operations
National Composites Centre
Bristol BS16 7FS, UK

The ORCID identification number(s) for the author(s) of this article can be found under https://doi.org/10.1002/mame.202400276

DOI: 10.1002/mame.202400276

fibers, fillers, particles, or flakes into polymeric materials stands out as a primary and efficient technique to enhance the integrity of polymeric components.[25–27] Bio-derived reinforcement, in particular, boasts superior biodegradability and lower density, thereby enhancing specific mechanical properties.[28–30]

Palaniyappan et al.[25] focused on developing FG composites using PLA and a novel extruded walnut shell particle reinforced through FFF technology. Various single and multi-gradient material deposition methods were employed, and their mechanical, thermal, and tribological properties were compared with standard 3D-printed PLA and walnut shell-reinforced PLA composites. Among the novel FG multi-materials (MM), the sample with a composite ratio of PLA (50%) and walnut shell reinforced PLA (50%) appeared suitable for semi-structural applications, while the composite (PLA of 40% as inner core) was recommended for highly wear-resistant constructional building panels for thermal proofing applications. Bodaghi et al.[9] studied adaptive metamaterials by FG FFF 4D printing. They used FFF 3D printing to create adaptive metamaterials. The key was understanding the thermo-mechanics of shape memory polymers. The material could be programmed to self-fold or self-coil by changing the printing parameters. This allowed for complex and intricate designs to be created.[31] Sun et al.[32] worked on 4D-printed materials with localized shape memory. They discussed utilizing FG layers to create localized actuation. The authors explored how different amounts of plasticizer could be used to achieve this. They found that tri-layer FG composites with increasing plasticizer content across the layers resulted in localized shape memory.

Moreover, Zeng et al.[33] investigated the fabrication of FG cellular structures incorporating a shape memory effect (SME) using 4D printing technology. They conducted experimental analyses and finite element simulations to assess the compressive performance and shape memory behavior of FG structures under different temperatures. The findings reveal that as gradient parameters increased, the maximum energy absorption gradually decreased while the compressive modulus steadily increased. The compressive modulus and strength of 4D printed FG structures declined as temperature rose due to the influence of shape memory polymers, yet they exhibited remarkable shape recovery capability when subjected to high-temperature stimuli. Rahmatabadi et al.[34] introduced the novel approach of 4D printed bilayer-encapsulated polycaprolactone (PCL)–thermoplastic polyurethane (TPU) SMPC structures, employing dual-material extrusion printing. The results demonstrated encapsulation enhanced SME performance compared to bilayer PCL–TPU structures. Furthermore, experiments revealed that maximum stress recovery in 4D-printed composites remained consistent over time, a significant improvement over previous extrusion-based SMPC structures which often suffered from weaknesses in stress relaxation due to weak and low crystalline fractions, and the unravelling of molecular entanglements in semicrystalline and amorphous thermoplastic SMPCs.

Prior research has thoroughly explored the advancement and evaluation of SMPCs, FFF 3D/4D printing, and MM and FG 4D printing with reinforcement from natural fibers or particles. However, these investigations have primarily focused on using FG to enhance the mechanical properties of printed structures. However, it is crucial to emphasize that these earlier investigations have often neglected a significant aspect which is the combination of FG biodegradable biocomposites through 4D printing. Meanwhile, the literature review revealed minimal research efforts in the development of diverse 4D-printed FG biocomposites for use in different applications.

Table 1. Physical properties of MPLA and WPLA.

Physical properties	MPLA	WPLA
Specific gravity [g cc]	1.24	1.24
Relative viscosity	4.0	4.0
Clarity	Transparent	Transparent
Peak melt temperature [°C]	145–160	145–160
Glass transition temperature [°C]	55–60	55–60

This study explores unique 3D/4D-printed biocomposite materials made from mussel PLA (MPLA) and wheat PLA (WPLA), combined with MM and FG structures. The main goals are to understand the mechanical properties of these biocomposites and their MM and FG printing and to investigate the shape memory properties of printed SMPCs through hot programming. This involves analyzing flammability, microstructure, and mechanical properties of the printed SMPCs. This approach yields FG composites that are biodegradable, compostable, and eco-friendly, resulting in a final product that is both lighter and stronger. Additionally, the shape recovery feature enables the reusability of 4D-printed objects, aligning with circular economy principles for sustainability. This method minimizes material usage in printing while simultaneously enhancing mechanical strength. Moreover, shape fixity, shape recovery, and shape memory responses of FG- and MM-printed specimens are assessed under identical printing conditions. A detailed analysis of scanning electron microscope (SEM) and energy dispersive X-ray spectroscopy (EDS) images of fractured specimens, as well as the microstructure with integrated particles, is conducted. The findings highlight the potential of SMPCs to revolutionize fields such as bio-based products, actuators, human-material interaction, and complex structures.

2. Experimental Section

2.1. Materials

The application of FFF 4D printing can be used to create products with a variety of material qualities and multifunctional features by utilizing a range of thermoplastic filaments that were now available, some of which incorporate functional additive particles.[35] Through deliberate alteration of the print at specific locations, these qualities can be customized throughout the print. Francofil-made MPLA and WPLA filaments with a diameter of 1.75 mm were used in this study.[36] The presence of PLA resin has made the materials' physical qualities comparable. Values were shown in **Table 1** based on supplier data sheets. PLA serves as the foundation for MPLA and WPLA filament, which was blended with particles derived from mussel shells and wheat. In essence, waste mussel and wheat by-products were blended with PLA to craft enhanced biocomposite filaments. These materials were eco-friendly, sustainable, biodegradable, and compostable. They can be employed across a variety of applications, contributing to a more sustainable environment.[37–43] Additionally, PLA

Table 2. Printing parameters of MM/FG SMPCs.

Parameters	Value
Nozzle Diameter [mm]	0.6
Layer Thickness [mm]	0.2
Printing Speed [mm $^{-1}$s]	60
Infill Density [%]	100
Printing Pattern	Linear
Nozzle Temp. [°C]	190
Bed Temp. [°C]	60

was widely available and exhibits a large SME when compared to other widely recognized SMPCs. To evaluate the mechanical characteristics of MM and FG samples alongside pure PLA, pure PLA pellets from Resinex were acquired and transformed into 1.75 mm filaments using a 3devo filament maker.

2.2. Design and Printing

This section provides a comprehensive description of the production process for MM and FG SMPCs and introduces the FFF printers for printing structures. This study utilized a Geeetech A30M 3D printer. The printer's extruder was equipped to print both MM and FG structures specifically for this research endeavor as shown in **Figure 1**a. The extruder was responsible for simultaneously combining molten biocomposite plastics to enable their joint deposition later on (see Figure 1a). The proportion of molten plastics was varied between different samples by modifying the extruder speed, which dictated the filament feed rate. A blend of MPLA and WPLA materials was designed and printed using MM and FG printing techniques to achieve rapid and stable structures, along with 3D objects endowed with morphing capabilities.

All samples in this research were printed with uniform printing settings as detailed in **Table 2**. Samples were created using the extruder with a diameter of 0.6 mm, ensuring smooth production without encountering any clogging issues. The geometry of these prototypes was designed using SolidWorks software. Subsequently, the specimen's shape was saved as a stereolithography (STL) file and imported into the slicing program Cura, where processing settings were customized accordingly. For the MM and FG printing, ColourMixer software was utilized to print the specimens. The software enabled adjustments to the material flow and the proportion of material utilized in MM and FG printing. The layout depicting the printing of samples with FG and MM printing features was illustrated in Figure 1b. MPLA and WPLA samples were printed to form composite and sandwich composite structures with MM and FG components, aiming to investigate their performance.

2.3. Mechanical Properties

The mechanical characteristics of SMPCs were evaluated using a versatile mechanical testing apparatus, namely the Shimadzu AG-X plus machine, equipped with a 50 kN load cell. Specimen displacement was monitored utilizing an optical camera during testing. The dimensions of the tensile specimens for all biocomposite samples adhered to the standards ASTM D638.[44] The samples were printed vertically (build orientation of 90°) to explore the effects of MM and FG printing on mechanical properties. The testing was conducted at a speed of 5 mm min^{-1}. Additionally, samples were manufactured to assess their characteristics through three-point bending and compression. The dimensions of the compression specimens were consistent with ASTM D695 standards, with a testing speed of 5 mm min^{-1}.[45] The dimensions of the bending specimens, printed horizontally, were dictated by ASTM D790 standards, with a testing speed of 5 mm min^{-1} and a span length of 40 mm.[46] The desired qualities were tested on a total of five samples, and the average values for each parameter and standard deviation were subsequently presented. Figure 1c depicts both the test specimens and the final printed samples in a random arrangement. The diagram illustrating printed FG specimens and the executed examinations was depicted in **Figure 2**a. The primary objective was to produce FG samples where the exerted force aligns with the graded or multiple layers. The stress and strain were calculated in Equations 1 and 2 based on ASTM D790 as follows:

$$\sigma_f = \frac{3FL}{2bd^2} \tag{1}$$

$$\epsilon_f = \frac{6Dd}{L^2} \tag{2}$$

Here, σ_f was stress, ϵ_f was strain, b was the test sample width, d was the sample thickness, F was the force causing the bending, L was the distance between the supports, and D was the maximum deflection of the beam's center.

2.4. Dynamic Mechanical Analysis (DMA)

The storage modulus and the glass transition temperature (T_g) were two crucial thermodynamic factors that were intimately related to the SME of 4D-printed SMPCs. It was necessary to consider several parameters before evaluating the material's shape memory behavior. Analysis of the effect of natural particle integration on the semi-crystalline PLA's storage modulus and T_g was required. In this study, dynamic thermomechanical analysis on 4D-printed MPLA, WPLA, MM-printed, and FG-printed specimens, all printed vertically, was conducted using a dynamic thermo-mechanical analyzer (PerkinElmer DMA 8000). The dimensions of the printed beam samples were 30 mm in length, 10 mm in breadth, and 1.8 mm in thickness (see Figure 1c). A standard frequency (1 Hz) and heating rate (5 °C min^{-1}) were used, with specimens tested between 30 and 80 °C.

2.5. Scanning Electron Microscope (SEM) and Energy Dispersive X-Ray Spectroscopy (EDS)

An SEM (JSM-7100 F LV FEG) was employed to examine the phase structure of the SMPCs and assess the fracture of printed biocomposite structures. Following the tests, the interface shapes and broken cross-sectional views of the printed samples were analyzed. This investigation aimed to evaluate the overall bonding

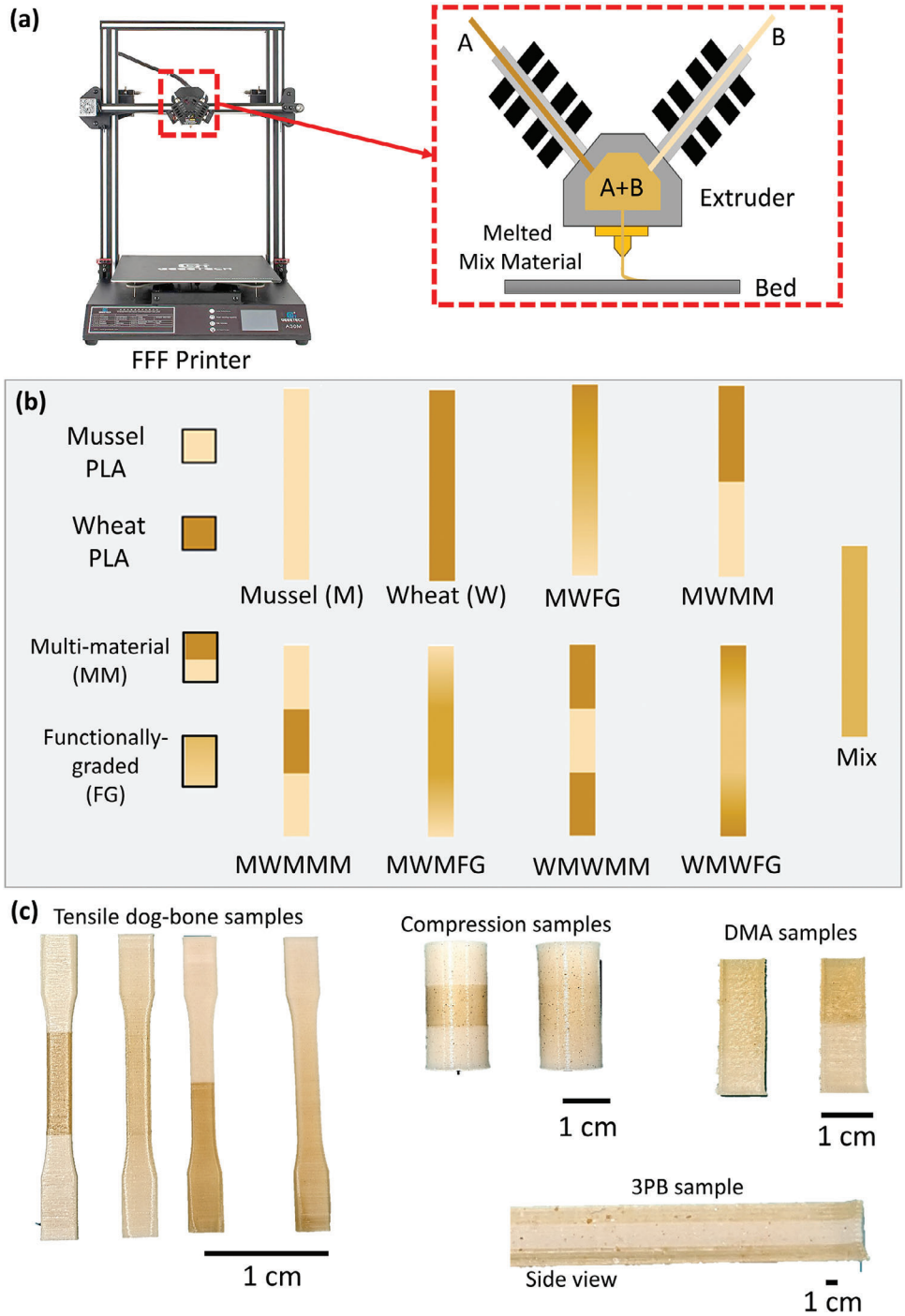

Figure 1. a) The schematic includes an example of printing composite specimens as well as a diagram of an FFF printer and its nozzle used to print MM/FG SMPCs. b) The schematic of the printed FG and MM layers used in structural printing. c) Photographs of samples and SMPCs that are manufactured following ASTM guidelines for mechanical tests.

strength of the printed composite and the effectiveness of the integration of the individual components. Also, EDS from Oxford Instruments was utilized to conduct surface elemental analysis, aiming for a semi-quantitative assessment of chemical composition. This analysis specifically targeted the bonding between the printed MPLA and WPLA to assess particle distribution.

2.6. Shape Memory Properties

The recovery of printed sample shapes under thermal stimulation was assessed using the hot programming technique. In order to examine the SME of the printed samples, SolidWorks was used to carefully design each specimen. These specimens were

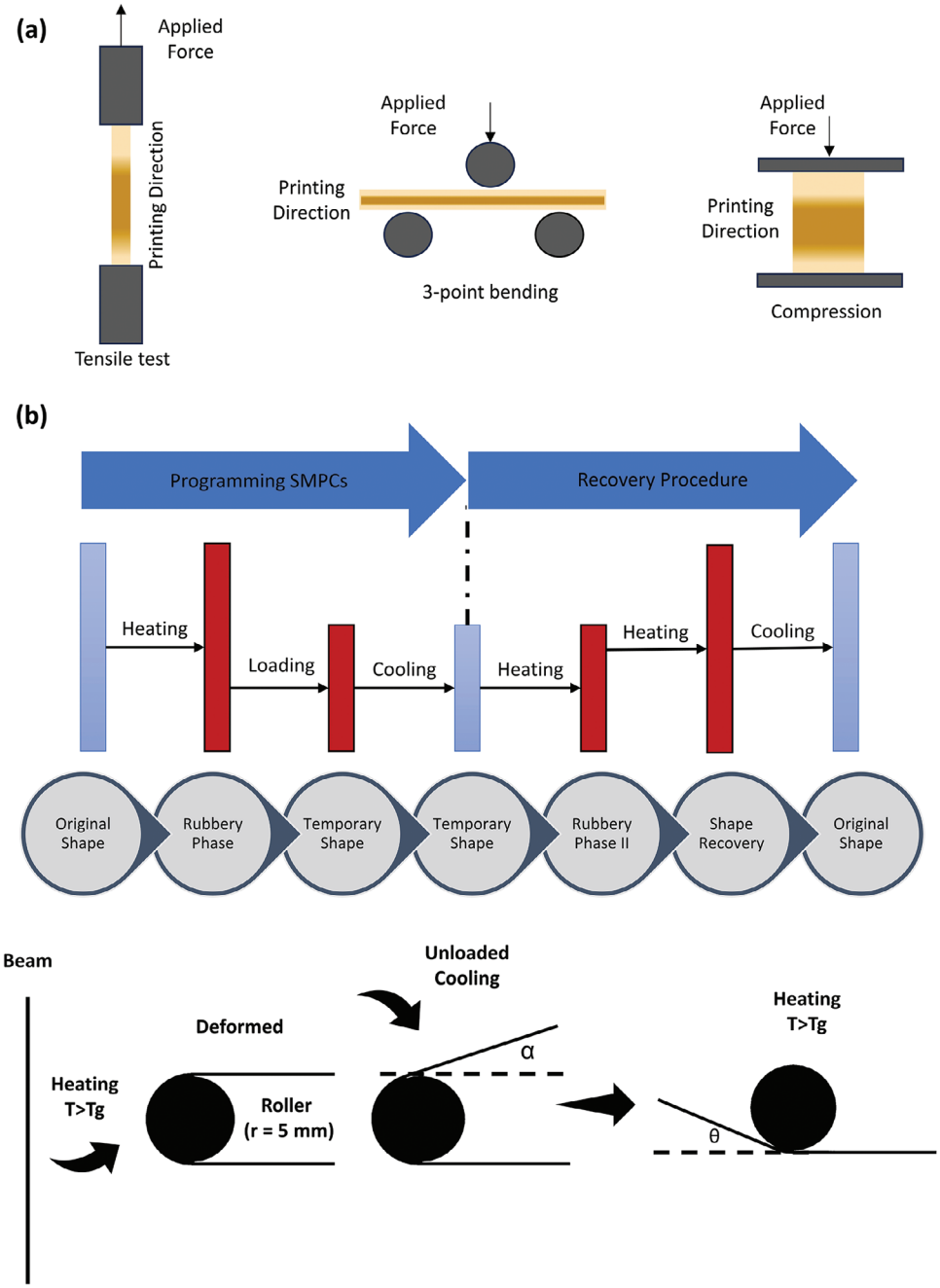

Figure 2. a) The mechanical test diagram for each printed MM and FG specimen. b) The method of configuring the SMPCs in hot programming. The procedures for programming and recovering in hot programming.

made out of MM and FG beams that were 70 mm long, 5 mm wide, and 2.5 mm thick. Examining the impact of particles on the PLA matrix's SME was the main goal. A set of 10 samples was tested for all printed biocomposites respectively. The detailed step-by-step instructions for programming SMPCs were shown in Figure 2b. Using a temperature-controlled heat gun that was set above the T_g, hot programming was used to distort the specimens. The specimens were chilled after deformation to guarantee shape stability. Then, beams that were programmed by hot procedures were heated over T_g to return to their initial shapes.

Equations 3 and 4 can be employed to calculate the shape fixity and recovery ratio, respectively.[47]

$$R_f = \textit{Shape fixity ratio} = \frac{\theta_{deformed} - \alpha}{\theta_{deformed}} \times 100\% \quad (3)$$

$$R_r = \textit{Shape recovery ratio} = \frac{\theta_{deformed} - \theta_{unrecovered}}{\theta_{deformed}} \times 100\% \quad (4)$$

In this context, the residual deformation of the sample that remains unchanged after the application of a stimulus was denoted as the angle $\theta_{unrecovered}$. The maximum angle to which the sample was distorted and temporarily held in place was represented by $\theta_{deformed}$ (refer to Figure 2b, unloaded section). During the experiment, mean values for both angles were calculated. The beams were fixed at one end and positioned vertically. Heating was performed using a heat gun at a specified temperature. The sequence of shape recovery was recorded and documented using a camera, PASCO software, and FLIR E5-XT thermal imager from FLIR. Additionally, a Keithley 2110 bench multimeter equipped with a wired thermocouple was utilized to measure the temperature of the beams during the shape restoration process.

2.7. Flammability

Flammability assessments in accordance with the ASTM D635-22 for determining the burning rate and/or extent and duration of burning of plastics when placed horizontally were conducted.[48,49] Horizontally mounted printed MM and FG strips in a fumehood were placed, marked at 25 mm and 100 mm from one end. The samples were printed vertically, resembling tensile test specimens, to assess their flammability. A gas torch flame was used to apply heat to the end of the strip, penetrating to a depth of 6 mm, and timing commenced simultaneously. The time and distance of the flame's progression, from the 25 mm mark to the 100 mm mark, were documented. The burning rates of the composites were determined using the following Equation 5.[50,51]

$$V = \frac{60L}{t} \tag{5}$$

In this equation, V represents the burning rate (mm min^{-1}), L denotes the burned length (mm), and t stands for the time of burning (min).

3. Results and Discussion

3.1. Mechanical Properties

The effectiveness of the created MM and FG specimens and the behavior of particles in SMPCs are assessed through the fabrication of standard tensile, compression, and bending test samples. These samples utilize pure PLA as well as MPLA and WPLA augmented with particles. For the tensile test, we employed vertical printing to illustrate the efficacy of FG printing by producing dog bone specimens. Naturally, PLA printed horizontally exhibits greater strength and rigidity compared to the vertical orientation. However, the primary focus remains on MM and FG printing.[52]

Figure 3a displays tensile test results for printed samples following ASTM D638 standards. All samples were printed under identical conditions. The findings suggest a significant strength improvement with FG printing, such as a 41% increase in strength in MWFG compared to MWMM printing. Furthermore, the WMWFG specimens, resembling a sandwich composite structure, exhibit superior properties with an average ultimate stress of 31.6 ± 1 MPa. The strength of the dogbone specimen's gauge section is attributed to a blend of wheat and mussel shell. The higher proportion of mussel in WMWFG samples leads to its increased tensile strength compared to other specimens. Additionally, the maximum stress value depicted in Figure 3d for printed MWMFG samples closely approaches that of MPLA. Nevertheless, it is important to acknowledge that the samples tend to develop cracks earlier because of the weaker bonding between MPLA and WPLA in MM specimens. This investigation into SMPCs versus pure PLA demonstrates that the incorporation of particles leads to a substantial enhancement in their mechanical properties. In contrast, specimens fabricated using MM printing exhibit reduced strength attributable to insufficient interlayer and intermaterial adhesion. Removing the vulnerable interface allows FG specimens to achieve improved stress distribution and increased overall strength. Meanwhile, a blend of MPLA and WPLA (Mix sample) yields an average result of 19.2 Mpa, which is representative of the average outcome between MPLA and WPLA. In general, FG-printed specimens exhibit enhanced mechanical properties when compared to MM printing.

In addition, three-point bending tests were used to see how MM and FG samples behave under bending forces (see Figure 3b). The samples were printed horizontally to investigate the properties of MM and FG printing. The aim of MM and FG printing horizontally is to align the applied force with the layer printing. The results from the three-point bending tests differ from the tensile tests; however, the FG specimens demonstrate superior properties compared to the MM samples. The thickness of the 3-point bending samples was 3 mm and the form of printing was different from tensile and compression tests. Compared to tensile and compression, where the samples were thicker in the printing direction, the combination of FG and MM was less effective. Also, The 3-point bending samples were likely to fail on the tension surface. Additionally, all MM and FG samples exhibit greater strength than the MPLA and WPLA materials. Among all specimens, the Mix and MWFG samples demonstrate notable strength, with average maximum stresses of 54.90 MPa and 54.09 MPa, respectively (see Figure 3d). In a compression test, the highest stress is observed when the material reaches its maximum compressive strength at the elastic limit. The values are shown in Figure 3d in the form of scattered dots. Similar to the tensile test, pure PLA falls between MPLA and WPLA with an average value of 41.02 MPa. It shows that the average values of ultimate stresses are quite consistent across all mechanical tests for printed MM and FG specimens.

Compression tests were conducted on all samples as shown in Figure 3c. The results of the compression tests are consistent, with maximum stress fluctuating between 59 MPa to 73 MPa across the samples. The maximum stress is typically recorded when the material fails or reaches its maximum compressive strength (Elastic limit). The MWMFG samples exhibit superior strength with the value of 73.5 MPa among all samples, attributed to the higher strength of MPLA and enhanced interlayer bonding. In the sandwich WMWFG composite sample, the material is stiffer in the middle compared to the top and bottom. This is why there is an increase in strength after the first peak. Similar to the results observed in tensile and three-point bending tests, the results of compression tests indicate that FG specimens are stronger compared to MM samples.

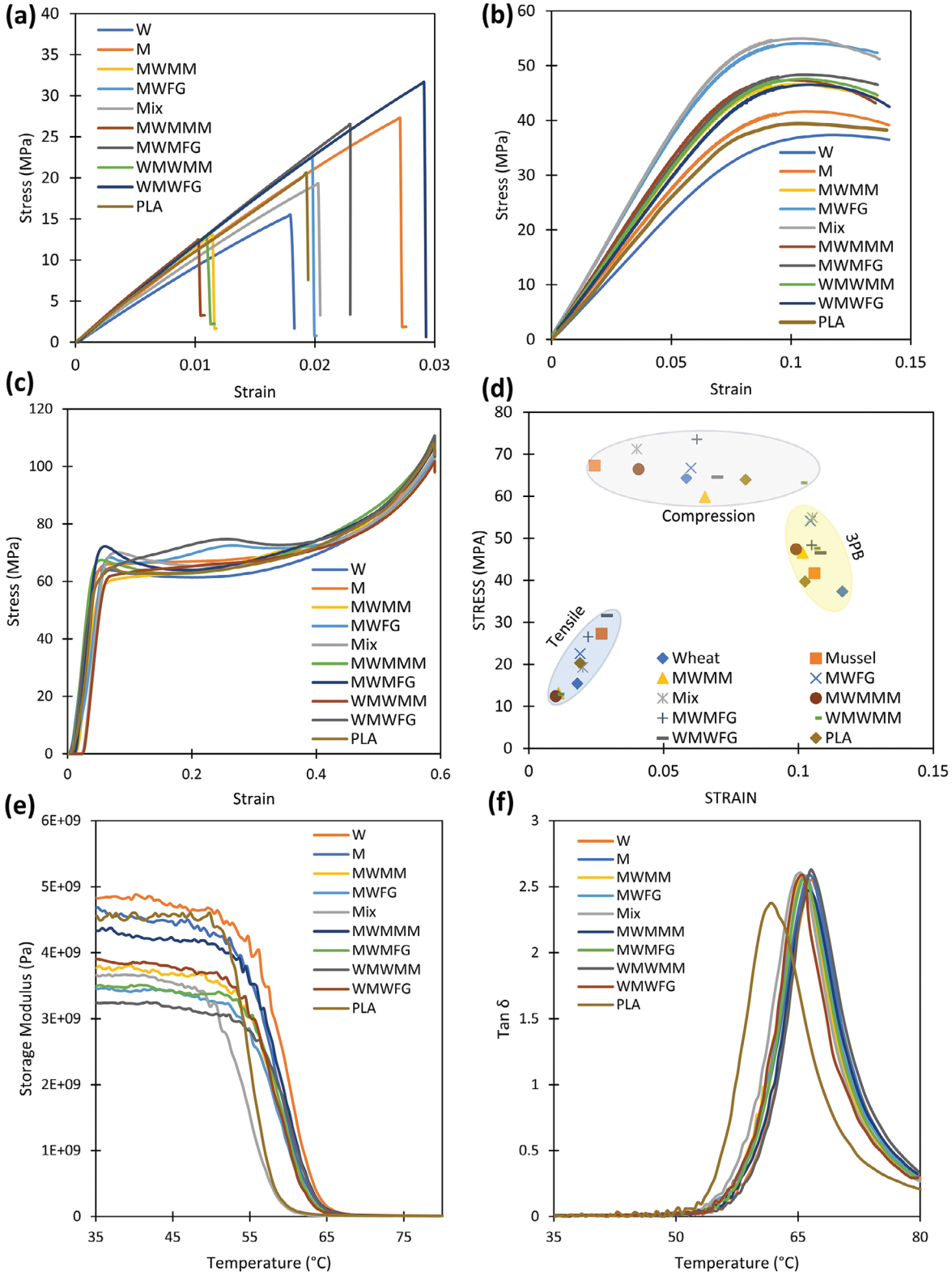

Figure 3. a) Median average results of tensile testing for printed samples by ASTM guidelines. b) Three-point bending test median average results for SMPCs. c) Compression test median average results for SMPCs. d) Median average maximum stress values determined by mechanical testing on printed SMPCs, e) and f) median average results from DMA for printed SMPCs.

In MM samples, abrupt transitions between distinct layers or phases can act as stress concentrators, ultimately leading to premature failure. FG samples address this issue by employing a gradual stress in material composition. This creates a smooth interface between regions with differing properties, thereby promoting a more uniform distribution of stress throughout the material. Consequently, FG structures exhibit enhanced mechanical integrity.[53] The mechanical results reported in this study indicate that reinforcing PLA with particles and printing FG composite sandwich products enhances both strength and stiffness. This has significant potential for real-world applications, especially in 4D printing, where it allows for creating various objects with less material without sacrificing strength. This innovation not only improves structural integrity but also significantly contributes to eco-friendly manufacturing.

To assess the shape memory characteristics of SMPCs to their mechanical properties, DMA testing was conducted on all printed composites using uniform size and printing conditions. Figure 3e,f display the storage modulus and tan δ values for both MM/FG SMPCs. The findings reveal a significant difference in the storage modulus of SMPCs. Also, the tan δ is different in printed samples, attributed to the relatively rigid nature of printed SMPCs. Consequently, the inclusion of particles notably enhances the stiffness, strength, and overall mechanical properties of the PLA matrix. Meanwhile, the storage modulus of MM and FG samples is lower compared to the WPLA and MPLA. The T_g of composite samples is between 66 to 67 °C. Furthermore, to ensure consistent results in shape memory properties, all samples are tested at temperatures exceeding their respective T_g values.

3.2. Microstructure

The microstructure analysis of printed SMPCs is pivotal for comprehending their mechanical and functional properties. Through SEM imaging, the intricate internal structure, including porosity and interfacial bonding, can be elucidated with high resolution. Furthermore, EDS provides elemental mapping and quantification, crucial for understanding the distribution and interaction of constituents within the SMPCs. **Figure** 4a illustrates the printing trajectory of vertically printed samples, where the layers are discernible. The diminished strength of vertically printed specimens compared to horizontally printed ones is attributed to inadequate bonding between layers. When objects are printed vertically, each layer is placed on top of the previous one, and there's less surface area for adhesion between the layers. This can lead to weaker bonding between the layers, making the object more prone to breaking or snapping under stress. Additionally, voids become apparent along the side of the sample where the nozzle turns to complete the trajectory, contributing to reduced strength in the vertical printing of tensile dog bone specimens. Moreover, tiny cracks appear inside the layers. These cracks grow longer as the pressure increases. The distribution of particles is observable in both MPLA and WPLA specimens. For example, in Figure 4c, the distribution of K and Ca is depicted, showing their presence in specific areas. Furthermore, particle agglomeration occurs in specific areas. When particles aggregate, they generate regions of stress concentration, rendering the material more susceptible to failure under applied load.

To delve deeper into the particle/matrix bonding, the fracture surface of the SMPCs was dissected, and multiple photographs were captured using SEM (see Figure 4b). The printing direction is discernible along with particle distribution in the fractured parts of the specimens. Porosity and small cracks are also apparent, both of which adversely impact the mechanical properties.[54] This investigation reveals that porosity and cracks within a material act as stress concentrators, generating localized regions of heightened stress. As a direct consequence, these defects can lead to a reduction in strength, as the material exhibits increased susceptibility to failure under lower applied loads. Furthermore, the presence of such imperfections diminishes the material's stiffness, also known as its modulus, resulting in a propensity for greater deformation under stress. While cracks may contribute to a weakening effect, they can also, through mechanisms like crack deflection or bridging, enhance fracture toughness to a certain extent.

FG specimens demonstrate greater strength than their pure counterparts due to several key factors. The strength improvement observed in this experiment, where MPLA and WPLA are combined in an FG structure, can be attributed to several mechanisms likely working together within the composite in a synergistic manner. First, the gradual transition in composition between MPLA and WPLA fosters improved interface bonding, mitigating crack propagation and enhancing overall mechanical integrity. Additionally, the redistribution of stress within the FG structure helps to evenly distribute load, reducing the likelihood of failure. This optimized stress distribution, coupled with synergistic interactions between the constituent materials, can lead to superior mechanical properties such as increased strength and toughness. Moreover, the ability to tailor the microstructure and material properties of FG specimens allows for customization to meet specific performance requirements, further contributing to their enhanced strength in mechanical tests.

Additionally, the EDS examination was performed on both MPLA and WPLA to analyze their constituent elements. Figure 4c illustrates the outcomes for printed MPLA specimens. With carbon dominating at 52 wt% and oxygen following closely at 47 wt%, it's evident that both MPLA and WPLA component significantly contributes to the composition of the specimens. The presence of calcium at 0.6 wt% suggests the incorporation of mussel shell, a known source of calcium carbonate in MPLA. Additionally, the detection of organic potassium at 0.4 wt% hints at potential additives of MPLA. Meanwhile, WPLA is mostly made up of carbon (52 wt%) and oxygen (48 wt%). Wheat, a natural substance, has these elements mainly carbohydrates, proteins, and fats. PLA, a type of bio-derived polymer made from plants like corn or sugarcane, gets its structure from carbon and oxygen atoms linked together as long chains. The presence of gold in the EDS results of printed specimens is attributed to the application of a gold coating during sample preparation for electron microscopy analysis.

3.3. Shape Memory Properties

The shape memory performance of these PLA biocomposites was tested via the hot programming method outlined in Section 2.6. The aim is to explore how incorporating particles influences the

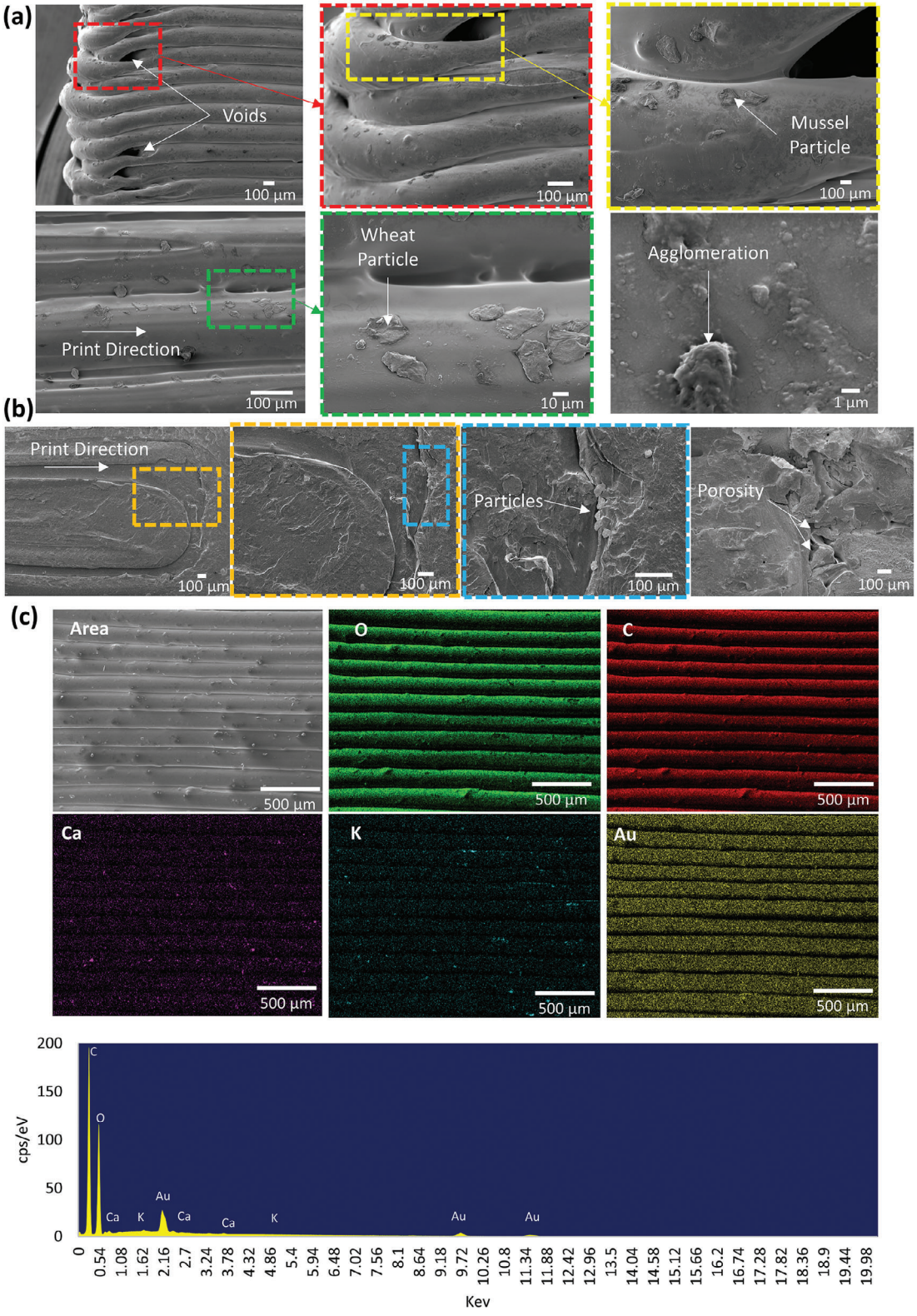

Figure 4. a) SEM images showing SMPC layer printing regions. b) SEM images showing SMPC failure areas. c) EDS results and images showing MPLA composite areas.

shape fixity and recovery of SMPCs. **Figure 5a** depicts the programmed shape and the resulting recovered shape in hot programming for the SMPC beam. To evaluate the shape memory behavior of the printed samples, they were gripped vertically. An infrared camera and a thermocouple were both used to capture temperature readings. The SME of the PLA matrix allows the sample to return to its original shape when exposed to heat from a heating gun at a specific distance. The sample exhibits a high degree of shape fixity due to the hot programming method. The infrared pictures clearly show the printed SMPCs returning to their initial form after heat treatment. Furthermore, the test involved recording sample trajectories throughout both the programmed and recovered phases. The trajectory programmed and recovered shape of the SMPCs under hot programming conditions is shown graphically in Figure 5b. In addition, a thermocouple was used to monitor and verify the experimental data. The sample is regarded as a material with one-way shape memory.

Figure 5c shows the time sensitive nature of temperature measurement. The high rate of heating was employed to accelerate the shape recovery process, minimizing the duration of heating for the samples. A detailed performance evaluation of printed SMPCs was carried out. The ratios that show how much the shape is maintained for beams that are programmed are shown in Figure 5d. Applying hot programming yields a significant improvement in shape stability. The shape fixity of all SMPCs and sandwich beams was documented to be between 98% to 100%. In hot programming, the ability to maintain shape rises in SMPCs.[47] MWFG has the best capacity to hold its shape out of all of these materials, while WMWFG comes in second in hot programming. The least capacity to hold their shape is shown by the MPLA printed beams.

The shape recovery ratio of printed SMPCs is also shown in Figure 5e. Collected data was based on a collection of ten specimens. The most remarkable shape recovery is found in beams made entirely of WPLA, which achieves a recovery ratio of 93.3% in hot programming. With 91.2% shape recovery in hot programming, the sandwich WMWFG composites come in second place; however, the shape recovery ratio of all composites is similar. The discrepancy results from the stiffer MPLA compared to WPLA. Also, the shape recovery performance of printed Mix beams is the lowest among all printed samples due to the higher strength as stated in the 3-point bending test. Additionally, the findings indicate that the FG specimens exhibit a superior shape recovery ratio in contrast to the MM samples. PLA's form recovery abilities are drastically reduced when particles are added. The shape recovery capability of printed SMPCs is reduced when particles are incorporated.

The fundamental structural features of natural particles in printed PLA can impede shape recovery. These particles add a degree of stiffness and hardness to the PLA matrix that could compromise the polymer's greater flexibility.[55,56] This disparity in material behavior may cause the composite's overall elasticity to decrease, making it more difficult for the material to regain its original shape after deformation. The interaction between these particles and the polymer matrix might not be uniform, resulting in inconsistent behavior. Further hindering shape recovery is the possibility of localized stress concentrations in the material caused by misaligned or unevenly distributed particles. Additionally, the bonding strength between the PLA matrix and the particles is very important. The optimal performance of particle-reinforced printed PLA biocomposites requires careful consideration of various factors, such as particle type, orientation, concentration, and processing techniques.

As shown in Figure 5f, a shape recovery test utilising cycles of hot programming was conducted. The SMPC samples used in this test resemble printed beams. These specimens went through twenty cycles of alternating programming. WPLA phases exhibit a consistently higher shape recovery, i.e., they more easily return to their original form. On the other hand, the shape recovery ratio is marginally lower for WMWFG. Whereas Mix samples perform worse in the cyclic test during the hot programming phase. To sum up, after WPLA samples, sandwich WMWFG performs better than other MM and FG samples in terms of shape recovery as well as cyclic shape recovery. Programmability in SMPCs is typically influenced by factors such as the material's ability to undergo reversible phase transformations or recoverable deformation under certain conditions like temperature or stress. Various defects, including microstructural flaws or chemical bonding, could contribute to the material's strength and shape recovery behavior. This could help elucidate whether the observed correlation between strength and programmability is indeed causal or if other factors are at play. For instance, defects such as poor bonding between WPLA and MPLA particles may be the cause of the poor shape memory and hot programming observed in the FG and MM samples. Future research could involve morphological tests and chemical property investigations to gain a deeper understanding of these issues.

3.4. Flammability

Figure 6 illustrates the average burning rates of the composites as determined by the horizontal burning test. All of the samples were burned completely and showed a burning rate much lower than pure PLA.[57] Among the samples tested, the WPLA composite exhibits the highest burning rate. This heightened rate in the WPLA sample can be attributed to its significant cellulose content compared to other hybrid composites, indicating a greater susceptibility to flames. Also, the rapid thermal degradation of PLA during combustion led to the poor flammability behavior observed in the WPLA sample. On the contrary, Figure 6 indicates that MPLA samples have the lowest average burning rate among all specimens and show 58% improvement compared to pure PLA. In terms of composites, MPLA demonstrates a reduced burning rate due to the mussel shell powder content. This effect is likely due to particle formation, which acts as a barrier, preventing heat and volatiles from penetrating the inner layers of the composites.[50,51] The burning rate of other specimens varies between the maximum peak burning rate of MPLA and the maximum peak burning rate of WPLA.

4. Applications

4.1. Bio-Based Products

Utilizing 3D/4D printing technology and bio-based reinforcement reduces the energy expended in the development of biocomposites, from raw materials to final products. Today, there is

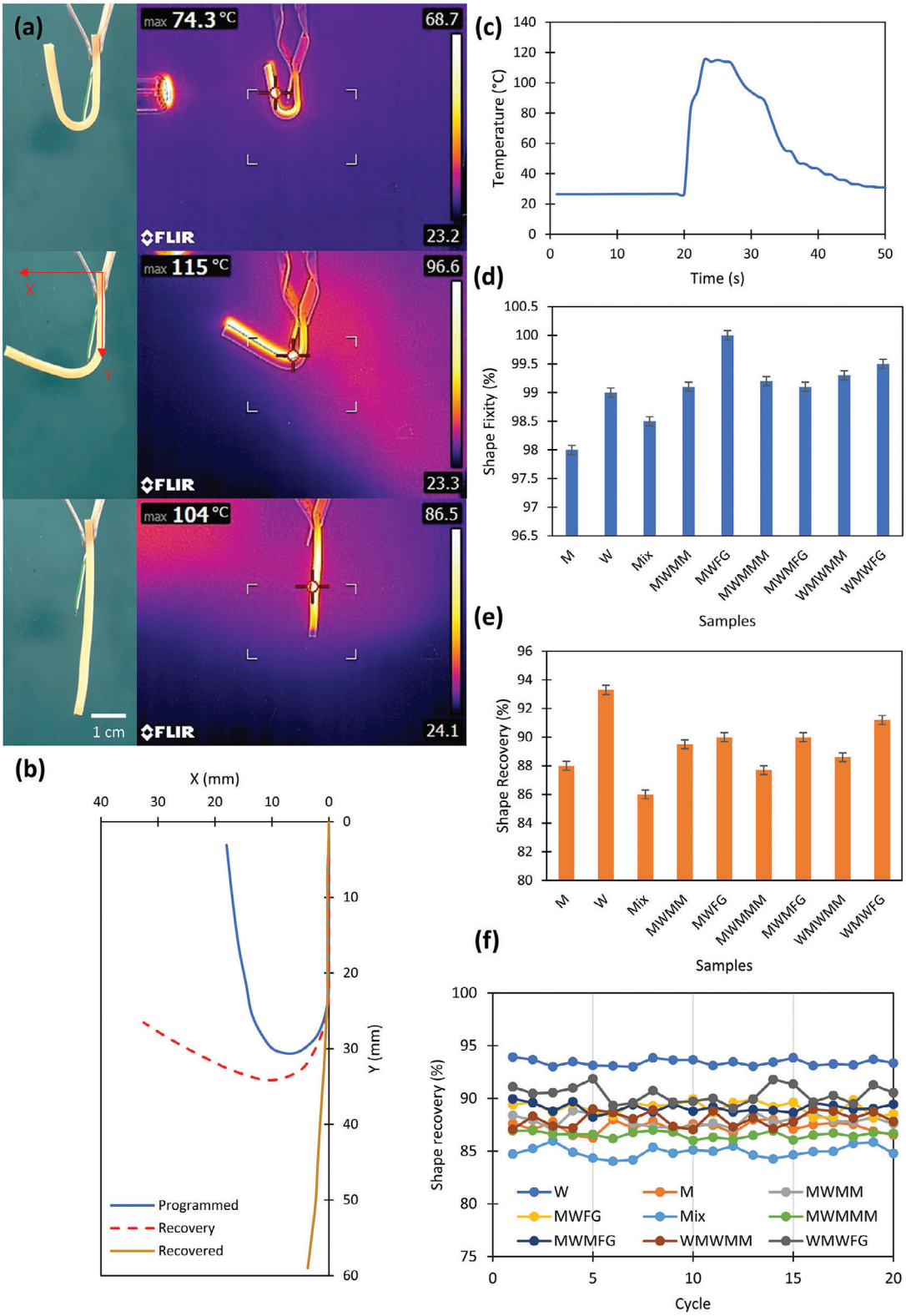

Figure 5. a) The programmed printed biocomposite beam's fixed shape and recovered shape are shown with infrared images at the beginning and end of the cycle. b) The programming-based projection of a composite beam's fixed and recovered shape. c) Temperature monitored in programming during the shape recovery process using a thermocouple. d) Shape fixity ratio for printed SMPCs. e) Shape recovery ratio for printed SMPCs. f) Hot programming's cyclic shape recovery ratio.

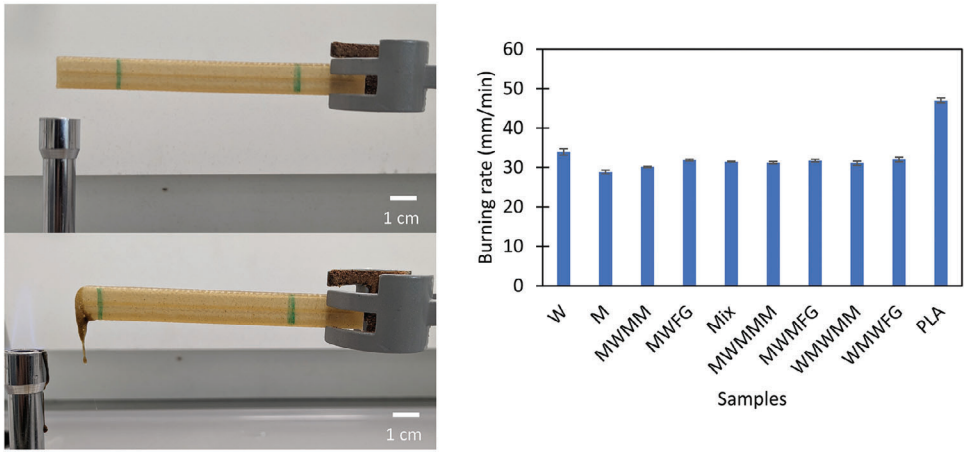

Figure 6. Visual documentation of clamping specimen and igniting it. The burning rate assessment of printed MM and FG composites.

a demand for diverse end products to fulfil human needs. A variety of concepts and end products are custom-designed and manufactured through 3D/4D printing, utilizing design files tailored to individual requirements. In this study, bio-composites derived from FG structures are harnessed for the 3D/4D printing process to manufacture various items, capitalizing on their superior mechanical properties and shape memory characteristics.

Lately, there has been a continuous interest in 3D/4D printing in the context of human-material interaction.[10,58,59] The significance of design principles facilitating the development of environmentally friendly 3D/4D-printed objects is emphasized, particularly in reducing material usage and waste. The innovative approach of utilizing 3D printing to craft MPLA or WPLA cutlery marks a significant leap towards sustainable dining solutions. By incorporating bio-based materials like MPLA derived from mussel shells, these utensils offer an eco-friendly alternative to traditional plastic cutlery, significantly reducing environmental impact (see **Figure** 7a).[60,61] The compostable nature of MPLA ensures that once disposed of, these utensils can be naturally degraded, minimizing waste accumulation in landfills. Moreover, the biodegradable properties of this material contribute to the preservation of marine ecosystems by avoiding the release of harmful microplastics. However, the use of bio-based PLA might have the risk of allergies. This fusion of technology and nature not only addresses environmental concerns but also promotes a healthier approach to everyday dining practices.

Additionally, different concepts were developed with a focus on human-material interaction. The design concepts presented in this article stand out for their reusability, lightweight structure, and durability, all thanks to the integration of FG structures. The concept of 3D/4D printing a flat sheet that can be transformed into complex shapes presents a remarkable innovation in material efficiency and versatility. As shown in Figure 7b by initially printing a flat sheet, material usage is reduced, minimizing waste and promoting sustainability. This MPLA flat sheet serves as a blank canvas, capable of being programmed through controlled heating to achieve complex shapes and shape morphing, such as miniature pots for indoor plants. The ability to transform from a two-dimensional form to a 3D structure offers immense flexibility in design and application. Moreover, on a larger scale, this technology can be employed to craft larger flower pots, providing a sustainable alternative to traditional ceramic or plastic options. One of the key advantages lies in the sheet's shape memory property, enabling it to recover its original form upon reheating, thus allowing for iterative reshaping and reprogramming. This dynamic capability not only enhances production efficiency but also opens up new possibilities for customizable and adaptable shape-morphing objects in various domains, from household items to industrial applications. Crucially, this reprogammability presents new opportunities for reuse, potentially significantly extending the usable life of the products in question.

All of the subsequent design concepts and their shape programming are based on earlier research works.[9,62] Cross-shaped specimens crafted from the WMWFG actuator are introduced in Figure 7c. The shape-changing behaviour exhibited by these materials may revolutionize packaging structures through innovative 4D printing techniques. With a radius of 100 mm and a narrow 1.5 mm thickness, these specimens boast both structural integrity and versatility. These printed structures can be programmed to change shape during printing. When heated, they transform in a surprising way, gently wrapping around any objects placed inside them. The initial and final layers of printing are shown in Figure 7c. The printing parameters remained the same, except for the printing speed of the top layers, which is increased to 80 mm $^{-1}$s and a layer height of 0.1 mm. The material used for this concept was WPLA. An infrared camera records the heating phases as they occur, showing how the wrapping process gradually takes shape. The dissimilarities in the arms of the wrapping process are primarily attributable to the challenges associated with achieving integrated heating throughout the entire structure. This dynamic functionality not only ensures secure and snug packaging but also highlights the adaptability and efficiency of the WMWFG actuator in modern manufacturing and logistics. The combination of 3D/4D printing with bio-based materials, as outlined in this work, demonstrates how novel materials and manufacturing can facilitate eco-friendly design. These programs show a growing commitment to minimizing environmental impacts while maximizing efficiency and usefulness. The search for innovation is unwavering despite the inherent complications and difficulties, such as uneven material distribution and heating anomalies.

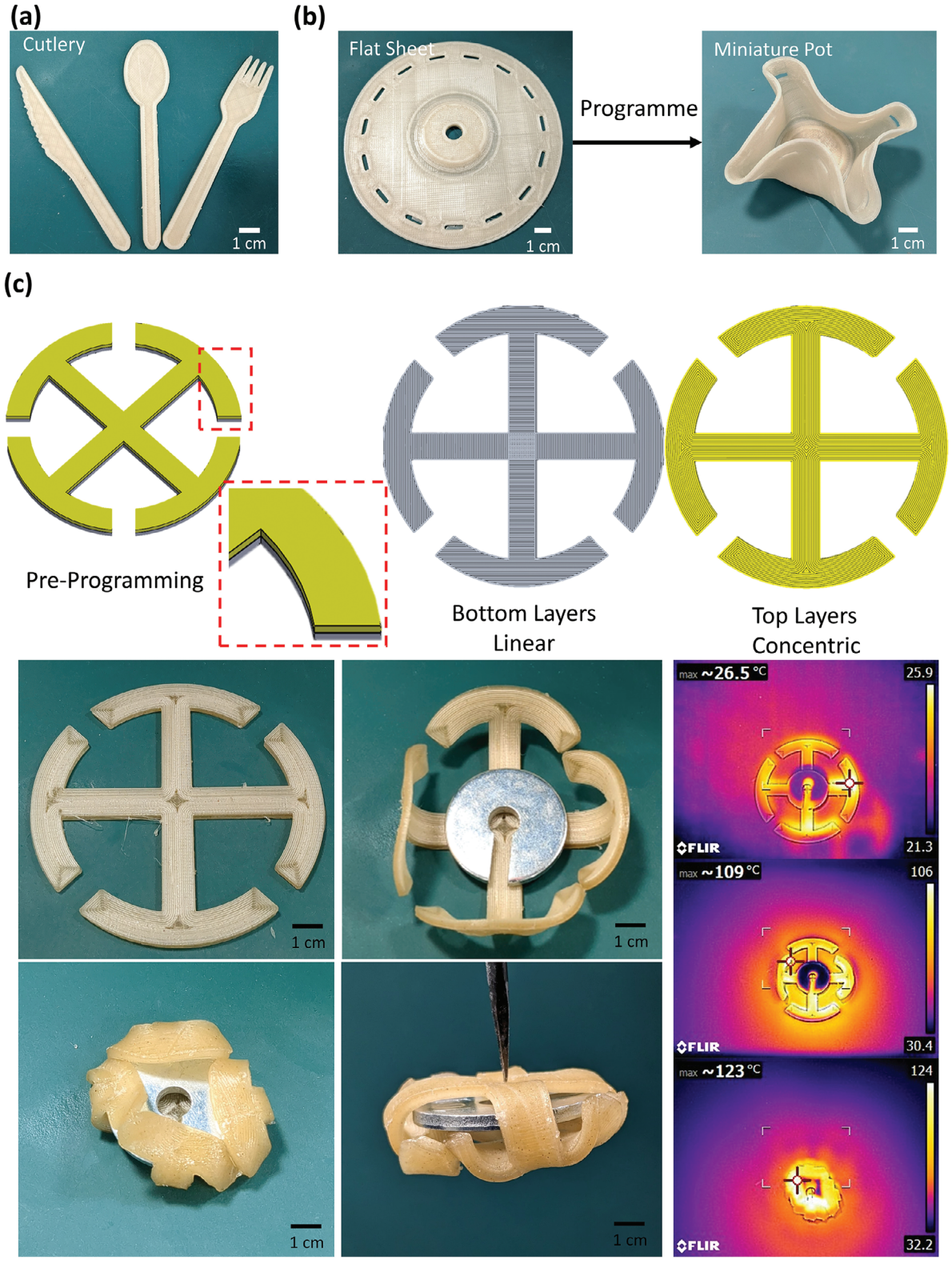

Figure 7. a) Printed MPLA for cutlery. b) Printed MPLA or WPLA flat sheet programmed to achieve complex morphing, creating miniature pots. c) Printed cross-shaped structure designed for wrapping and packaging, demonstrating step-by-step heating and shape transformation process.

4.2. Shape Morphing Holder

A novel shape-morphing design is depicted in **Figure 8**, taking the form of a rectangle and revolutionizing the possibilities of programmable 4D printing. This approach overcomes traditional manufacturing constraints by creating complex 3D lattice structures from simple 2D geometries using advanced programming techniques. Unlike conventional 3D printing methods that often require support to build designs, this shape-morphing approach eliminates the need for such structures, thereby streamlining the fabrication process and minimizing material waste.[43] Figure 8 visually demonstrates the design's transformative potential. It depicts the initial flat sheet undergoing a sequential transformation into a lattice structure. A printing temperature of 190 °C, a printing speed of 70 mm $^{-1}$s, and a printing layer height of 0.1 mm were used.

The MWMFG morphed shape structure, despite its lightweight nature of 5.30 grams, boasts remarkable strength and versatility, capable of supporting substantial weights both vertically and horizontally. In vertical orientations, this innovative design demonstrates impressive load-bearing capabilities, supporting a static mass of up to 3 kg without failure. Even when loaded horizontally, it maintains its structural integrity, able to sustain loads of 500 grams or more. This strength-to-weight ratio makes it suitable for a myriad of applications as concept, from shelving units to load-bearing components in various mechanical assemblies. Furthermore, when enlarged, this framework could be used to build a sturdy desk or stand, utilizing its rigidity and strength to offer reliable support for objects of different sizes and masses. The inherent stiffness of the structure ensures stability and endurance is increased by its complex lattice design, which optimizes loading distribution and prevents deformation. This amazing blend of sturdy performance and lightweight design highlights the revolutionary potential of shape-morphing technology, providing creative solutions for a range of home and industrial applications.

In addition to its impressive load-bearing capabilities, compression tests were conducted on samples of the lattice morphed shape structure to explore its force-morphing capabilities. Through controlled loading, a maximum force of 1100 N is achieved, as illustrated in Figure 8. This experimental validation further underscores the structural robustness and adaptability of this design, demonstrating its ability to withstand substantial forces while retaining its shape and integrity. This dynamic shape change highlights the inherent flexibility and adaptability of programmable materials, enabling the creation of intricate geometries that would be otherwise unattainable through conventional FFF 3D printing methods.[63] Moreover, the absence of support structure, which is normally used to print complex shape during FFF printing, not only enhances the efficiency of production but also ensures a more sustainable approach to fabrication, reducing resource consumption and environmental impact.

4.3. Actuator Gripper

A useful gripper concept is designed and developed in this section. As seen in **Figure 9**, the gripper design is a four-fingered structure printed in 2D with unique printing patterns that allow for a capturing motion. WMWFG printing was used to print the gripper. A printing temperature of 190 °C, a printing speed of 70 mm $^{-1}$s, and a printing layer height of 0.1 mm were selected. Figure 9 shows how the 2D structure undergoes a shape transition when applying heat, which enables it to grasp and retain an object. This gripper design is an excellent example of its adaptability in scenarios requiring good grabbing performance, simple transportation, and remote activation. It shows how 4D printing technology may be used in real-world applications. We anticipate several possible uses in robotics, automation, and material science—fields where flexible and programmable structures are indispensable—by using the shape-shifting qualities triggered by heat. Remote activation, in addition to enabling item transit and gripping, presents new possibilities for enhanced manipulation and handling in several industries.

5. Conclusion

This research proposed MM and FG 3D/4D printing of biodegradable MPLA and WPLA composites for enhanced flammability, mechanical and shape memory properties. This study also implemented programming approaches to accomplish the 4D printing of SMPCs. The results showed that FG samples perform better than MM samples in tensile, 3-point bending, and compression tests. Moreover, the strength was increased by combining the materials to create a sandwich FG composite structure, which is stronger than using pure WPLA or MPLA. The variable stiffness characteristic and SME of the 4D-printed SMPCs were assessed through DMA and heating-induced shape recovery tests, respectively. The DMA results show that the storage modulus of the printed FG and MM samples were different, indicating that the mechanical properties changed when printing with two different materials.

The shape memory properties of SMPCs were found to be less effective than those of pure PLA, even if their mechanical properties were significantly improved. In particular, the shape recovery ratios for WPLA beams were roughly 93.3%, 91.2% for WMWFG samples, and 86% for Mix samples. In addition, cyclic shape tests were performed for 20 cycles. Following a few cycles, the shape recovery ratio of SMPCs showed a modest fluctuation. A flammability test was performed to gauge the rate of combustion and the burn rate of the composite structure was consistently better than neat PLA. To illustrate the usefulness of 4D-printed SMPCs, FG samples were used to print products, grippers, and shape-morphing holders. Biocomposite consumer products were 4D printed with reusability features. One such example was a 4D-printed shape-morphed holder that can support loads up to 3 kg.

Further research on biodegradability, recyclability, and cyclic fatigue behavior of the materials and meta-structures could be carried out in the future to better understand their behavior under different conditions. This investigation would help identify the optimal parameters for printing meta-structures with MPLA and WPA materials. These findings would be instrumental for advancing the development and application of these materials in innovative structural designs. The proposed method of creating environmentally acceptable products through the use of bio-based natural composites would bridge the gap between technology and environmental awareness. By utilizing the adaptability of bio-derived materials in production processes, this innovative ap-

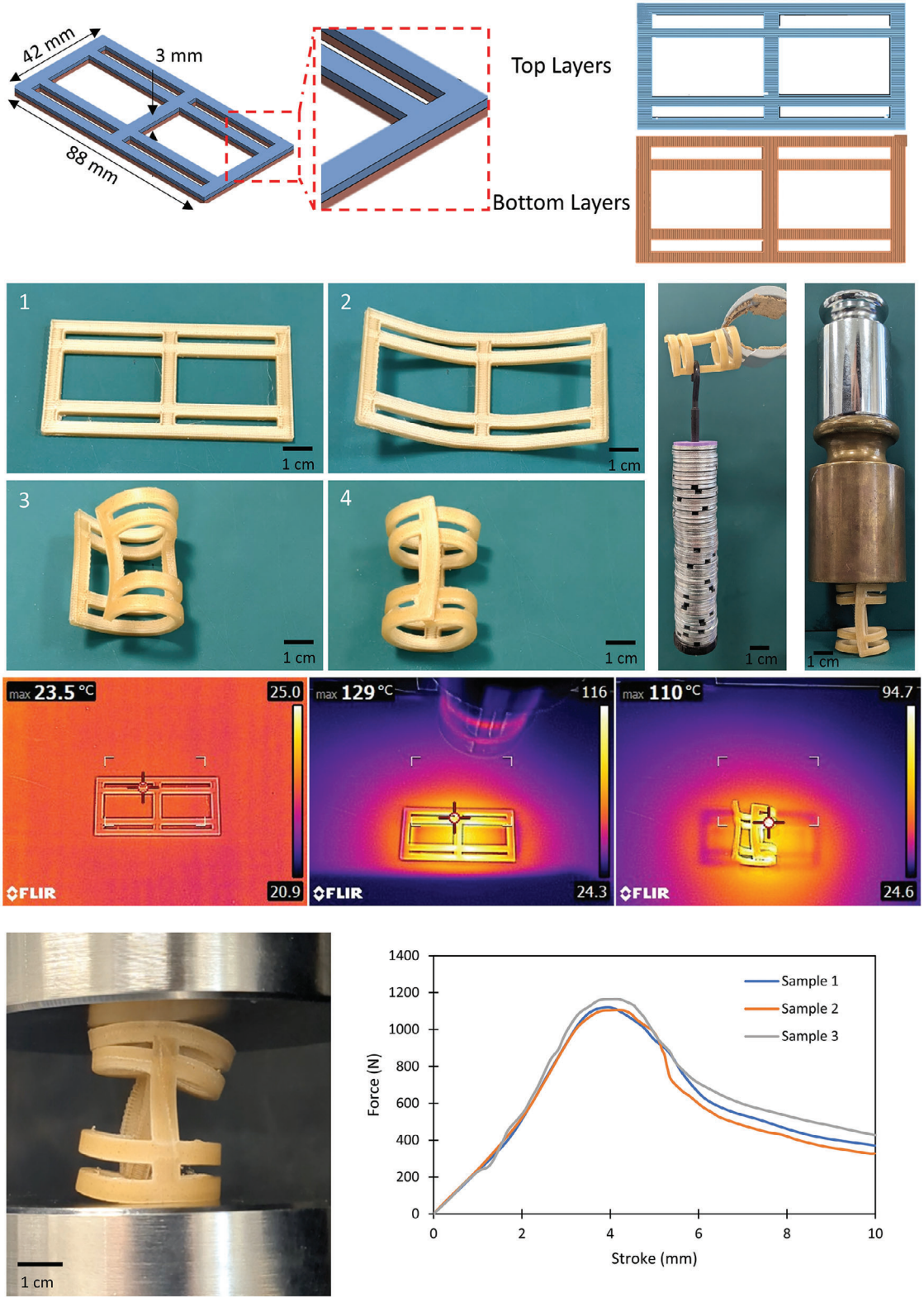

Figure 8. Printing of flat rectangular sheet and subsequent activation through shape morphing to achieve complex design. Weight and compression testing of the morphed structure to determine maximum force during morphing.

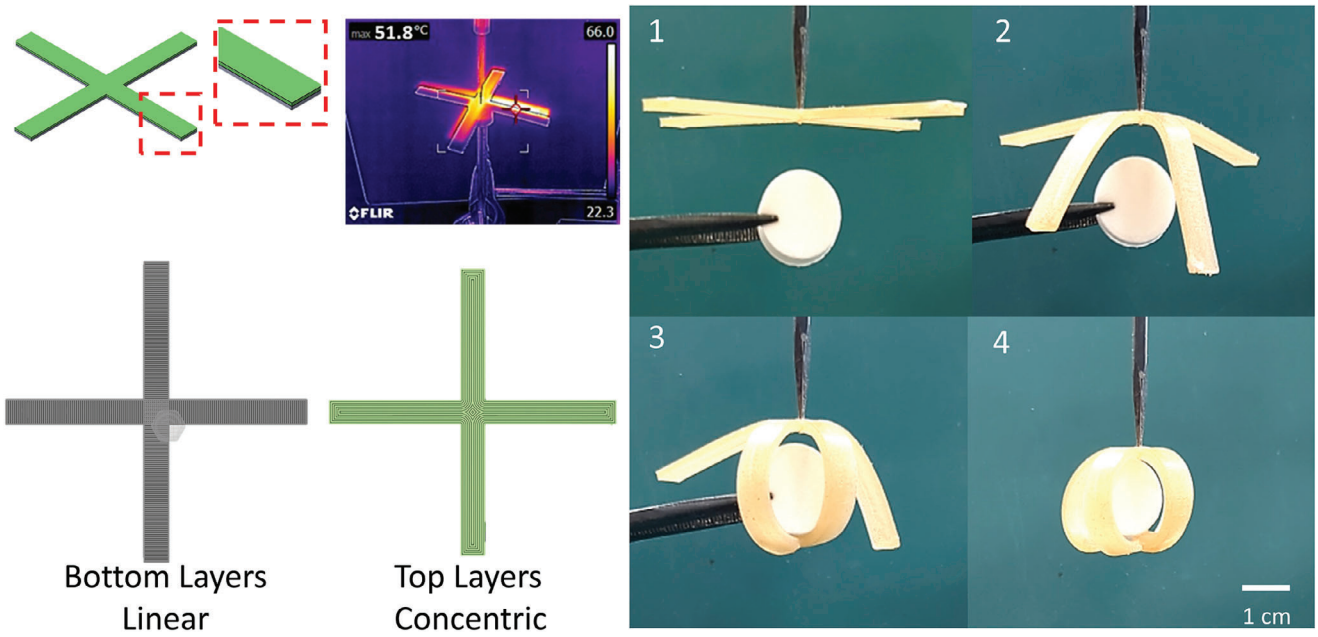

Figure 9. The functional gripper's schematic is designed with predetermined printing settings. The functional gripper's performance demonstrates holding an object by evolving its shape using heat.

proach would not only reduce dependency on synthetic materials but also promote a greener, sustainable future.

Acknowledgements

This project was a collaboration with the National Composites Centre (NCC), funded by the EPSRC's Innovation Launchpad Network+ Researcher in Residence scheme (Project: RIR26C230615-6, Researcher: Mahdi Bodaghi). The authors would like to acknowledge the use of the facilities in the 4D Materials and Printing Lab and the Imaging Suite in Medical Technologies Innovation Facility (MTIF) at Nottingham Trent University.

Conflict of Interest

The authors declare no conflict of interest.

Data Availability Statement

The data that support the findings of this study are available from the corresponding author upon reasonable request.

Keywords

3D/4D printing, biocomposites, fused filament fabrication, shape memory polymer composites, sustainability

Received: July 30, 2024
Revised: August 29, 2024
Published online:

[1] M. Lalegani Dezaki, M. K. A. Mohd Ariffin, S. Hatami, *Rapid Prototyp. J.* **2021**, *27*, 562.
[2] J. Carrell, G. Gruss, E. Gomez, *Rapid Prototyp. J.* **2020**, *26*, 855.
[3] M. Y. Khalid, Z. U. Arif, W. Ahmed, *Macromol. Mater. Eng.* **2022**, *307*, 2200003.
[4] L. P. Muthe, K. Pickering, C. Gauss, *Compos. Part C: Open Access* **2022**, *8*, 100271.
[5] M. Lalegani Dezaki, M. Bodaghi, *Int. J. Precis. Eng. Manuf. -Green Tech.* **2023**, *10*, 1661.
[6] H. Doostmohammadi, M. Baniassadi, M. Bodaghi, M. Baghani, *Macromol. Mater. Eng.* **2024**.
[7] E. Pei, G. H. Loh, D. Harrison, A. HdA, M. D. Monzón Verona, R. Paz, *Assembly Automation* **2017**, *37*, 147.
[8] M. Y. Khalid, Z. U. Arif, R. Noroozi, M. Hossain, S. Ramakrishna, R. Umer, *Int. J. Biol. Macromol.* **2023**, *251*, 126287.
[9] M. Bodaghi, A. R. Damanpack, W. H. Liao, *Mater. Des.* **2017**, *135*, 26.
[10] M. L. Dezaki, A. Zolfagharian, F. Demoly, M. Bodaghi, *Adv. Eng. Mater.* **2024**.
[11] M. Teacher, R. Velu, *Int. J. Precis. Eng. Manuf.* **2024**, *25*, 165.
[12] H. Liu, H. He, B. Huang, *Macromol. Mater. Eng.* **2020**, *305*, 2000295.
[13] Y. Li, Z. Feng, L. Hao, L. Huang, C. Xin, Y. Wang, E. Bilotti, K. Essa, H. Zhang, Z. Li, F. Yan, T. Peijs, *Adv. Mater. Technol.* **2020**, *5*, 1900981.
[14] M. K. Habibi, A. T. Samaei, B. Gheshlaghi, J. Lu, Y. Lu, *Acta Biomater.* **2015**, *16*, 178.
[15] G. H. Loh, E. Pei, D. Harrison, M. D. Monzón, *Add. Manuf.* **2018**, *23*, 34.
[16] X. Tian, Z. Zhao, H. Wang, X. Liu, X. Song, *J. Alloys Compounds* **2023**, *960*, 170687.
[17] I. M. El-Galy, B. I. Saleh, M. H. Ahmed, *SN Appl. Sci.* **2019**, *1*, 137810.
[18] K. Mirasadi, D. Rahmatabadi, I. Ghasemi, M. Khodaei, M. Baniassadi, M. Baghani, *Macromol. Mater. Eng.* **2024**, *309*, 2400038.
[19] J. Zhang, Z. Yin, L. Ren, Q. Liu, L. Ren, X. Yang, X. Zhou, *Adv. Mater. Technol.* **2022**, *7*, 2101568.
[20] S. Liu, Y. Li, N. Li, *Mater. Des.* **2018**, *137*, 235.
[21] R. Kumar, J. S. Chohan, R. Kumar, A. Yadav, S. N. Piyush, *J. Braz. Soc. Mech. Sci. Eng.* **2020**, *42*, 481.

[22] M. J. Mirzaali, M. Cruz Saldívar, A. Herranz de la Nava, D. Gunashekar, M. Nouri-Goushki, E. L. Doubrovski, A. A. Zadpoor, *Adv. Eng. Mater.* **2020**, *22*, 2070031.
[23] S. Hasanov, A. Gupta, F. Alifui-Segbaya, I. Fidan, *Compos. Struct.* **2021**, *275*, 114488.
[24] E. Soleyman, M. Aberoumand, K. Soltanmohammadi, D. Rahmatabadi, I. Ghasemi, M. Baniassadi, K. Abrinia, M. Baghani, *Manuf. Lett.* **2022**, *33*, 1.
[25] S. Palaniyappan, G. Annamalai, N. K. Shivakumar, P. Muthu, *J. Build. Eng.* **2023**, *65*, 105746.
[26] A. Le Duigou, D. Correa, M. Ueda, R. Matsuzaki, M. Castro, *Mater. Des.* **2020**, *194*, 108911.
[27] M. Y. Khalid, Z. U. Arif, A. Al Rashid, S. M. Z. S. Bukhari, M. Hossain, M. Koç, *Giant* **2024**, *19*, 100299.
[28] X. Song, W. He, P. Chen, Q. Wei, J. Wen, G. Xiao, *Polym. Compos.* **2021**, *42*, 899.
[29] S. Palaniyappan, D. Veeman, N. K. Sivakumar, L. Natrayan, *Structures* **2022**, *45*, 163.
[30] M. Kariz, M. Sernek, M. Obućina, M. K. Kuzman, *Mater. Today Commun.* **2018**, *14*, 135.
[31] M. Lalegani Dezaki, M. Bodaghi, *Int. J. Adv. Manuf. Technol.* **2023**, *126*, 35.
[32] Y. Sun, Y. Wan, R. Nam, M. Chu, H. E. Naguib, *Sci. Rep.* **2019**, *9*, 18754.
[33] C. Zeng, L. Liu, W. Zhao, Z. Liu, X. Xin, Y. Liu, J. Leng, *Sci. China Technol. Sci.* **2023**, *66*, 3522.
[34] D. Rahmatabadi, M. Aberoumand, K. Soltanmohammadi, E. Soleyman, I. Ghasemi, M. Baniassadi, K. Abrinia, M. Bodaghi, M. Baghani, *Adv. Eng. Mater.* **2023**, *25*, 2201309.
[35] K. Rajan, M. Samykano, K. Kadirgama, W. S. W. Harun, M. M. Rahman, *Int J. Adv. Manuf. Technol.* **2022**, *120*, 1531.
[36] Francofil. Francofil, https://francofil.fr/en/ (accessed: July 2024).
[37] V. Gigante, P. Cinelli, M. C. Righetti, M. Sandroni, L. Tognotti, M. Seggiani, A. Lazzeri, *Int. J. Mol. Sci.* **2020**, *21*, 5364.
[38] C. Cheng, Y. Chen, L. A. Kai-Xing, C. Yao, M. Shie, *J. Mater Sci: Mater. Med.* **2019**, *30*, 78.
[39] M. O. Lap, Y. Kanbur, Ü. Tayfun, *Chem. Chem. Technol.* **2021**, *15*, 621.
[40] C. Nyambo, A. K. Mohanty, M. Misra, *Macromolecular Mater. Eng.* **2011**, *296*, 710.
[41] N. Giani, L. Mazzocchetti, T. Benelli, M. Bovo, S. Gazzotti, D. Torreggiani, P. Tassinari, L. Giorgini, *Macromol. Symposia* **2022**, *405*, 2100235.
[42] E. H. Tümer, H. Y. Erbil, *Coatings* **2021**, *11*, 390.
[43] S. Ram Kishore, A. P. Sridharan, U. Chadha, D. Narayanan, M. Mishra, S. K. Selvaraj, A. E. Patterson, *Prog. Addit. Manuf.* **2024**, *9*, 37.
[44] ASTM International. ASTM D638-14, Standard Test Method for Tensile Properties of Plastics.
[45] ASTM International. ASTM D695-23, Standard Test Method for Compressive Properties of Rigid Plastics.
[46] ASTM International. ASTM D790-17 Standard Test Methods for Flexural Properties of Unreinforced and Reinforced Plastics and Electrical Insulating Materials.
[47] M. Lalegani Dezaki, M. Bodaghi, *Eur. Poly. J.* **2024**.
[48] B. Tawiah, B. Yu, B. Fei, *Polymers* **2018**, *10*, 876.
[49] ASTM. International. ASTM D635-22 Standard Test Method for Rate of Burning and/or Extent and Time of Burning of Plastics in a Horizontal Position.
[50] M. Azlin, S. Sapuan, M. Zuhri, E. Zainudin, I R. T Stability, *Polymers* **2022**, *14*, 2690.
[51] L. Lin, Q. A. Dang, H. E. Park, *Polymers* **2023**, *15*, 3270.
[52] N. H. Patadiya, H. K. Dave, S. R. Rajpurohit, Effect of Build Orientation on Mechanical Strength of FDM Printed PLA.
[53] S. Alkunte, I. Fidan, V. Naikwadi, S. Gudavasov, M. A. Ali, M. Mahmudov, S. Hasanov, M. Cheepu, *Comprehens. Rev. J. Manuf. Mater. Proc.* **2024**, *8*.
[54] P. H. M. Cardoso, R. R. T. P. Coutinho, F. R. Drummond, M. D. N. da Conceição, R. M. D. S. M. Thiré, *Macromol. Symposia* **2020**, *394*, 2000157.
[55] Y. Liu, W. Zhang, F. Zhang, J. Leng, S. Pei, L. Wang, X. Jia, C. Cotton, B. Sun, T. Chou, *Compos. Sci. Technol.* **2019**, *181*, 107692.
[56] Y. Wang, Y. Wang, Q. Wei, J. Zhang, M. Lei, M. Li, D. Li, *J. Polym. Res.* **2021**, *28*, 451.
[57] E. A. Franco-Urquiza, Y. R. Escamilla, *Polymers* **2021**, *13*, 3202.
[58] A. Zolfagharian, M. R. Khosravani, H. Duong Vu, M. K. Nguyen, A. Z. Kouzani, M. Bodaghi, *Polymers* **2022**, *14*, 3302.
[59] Y. Tao, S. Wang, J. Ji, L. Cai, H. Xia, Z. Wang, J. He, Y. Fan, S. Pan, J. Xu, C. Yang, L. Sun, G. Wang, presented at Proc. of the 2023 CHI Conference on Human Factors in Computing Systems Apr 19 **2023**, p. 1.
[60] M. Di Nicolantonio, E. Rossi, A. Vespoli, G. Annese Reusable Kit for 3D Printable Sustainable Cutlery.
[61] M. Garg, R. Rani, V. K. Meena, S. Singh, *Mater. Today Sustain.* **2023**, *23*, 100419.
[62] F. Wang, F. Luo, Y. Huang, X. Cao, C. Yuan, *Adv. Mater. Technol.* **2023**, *8*, 2201383.
[63] T. van Manen, S. Janbaz, K. M. B. Jansen, A. A. Zadpoor, *Commun. Mater.* **2021**, *2*, 1.

